The Structure of Supercritical Fluid Free-Jet Expansions

Imane Khalil and David R. Miller
Dept. of Mechanical and Aerospace Engineering, University of California at San Diego, La Jolla, CA 92093

DOI 10.1002/aic.10285
Published online in Wiley InterScience (www.interscience.wiley.com).

Experimental and numerical studies are reported on the structure of supersonic free-jet expansions of supercritical CO_2 impacting on a flat plate. Numerical calculations for the axisymmetric, two-dimensional (2-D) expansion use a time-dependent finite difference method known as the two-step Lax-Wendroff technique, incorporating the Redlich-Kwong equation of state to model CO_2. The numerical results are compared with experimental optical shadowgraph measurements of the jet and shock wave structure, impact pressure and temperature measurements along the plate, and a thermocouple probe of the expansion. Approximations based on ideal gases and quasi-1-D flow analysis, often used by researchers, are found to be useful for these supercritical fluid flows. © 2004 American Institute of Chemical Engineers *AIChE J,* 50: 2697–2704, 2004

Introduction

There has been considerable interest in the supersonic free-jet expansion of supercritical fluids (SCF) because of the role this rapid expansion plays in the decompression of high-pressure supercritical fluid mixtures. The rapid expansion of supercritical solutions (RESS) has been studied for nearly 20 years since the early articles of Smith and coworkers[1] to fabricate nanoscale particles, grow thin films, and as an interface to instrumentation, such as mass spectrometers and gas chromatographs. Several reviews[2,3] are available which describe the properties and uses of SCF. In our laboratory we are interested in using the properties of supercritical fluids to dissolve nonvolatile or temperature sensitive materials into a SCF and then to ultimately extract molecular beams from the free-jet expansions, which will permit us to examine the structure and chemical physics of small clusters. The high-pressure SCF mixture is decompressed typically through a narrow orifice or a long capillary tube. As the SCF flows through the orifice or tube, it accelerates in subsonic flow and reaches sonic conditions, Mach number equal to one, near the exit. The fluid then expands in a highly compressible, 2-D, supersonic, free-jet expansion, terminated by shock waves as the fluid pressure adjusts to ambient conditions. These free-jet expansions have been well studied for ideal gases and utilized by molecular beam researchers for more than 40 years.[4] The purpose of this research is to theoretically and experimentally examine the structure of the free-jet expansion for a SCF.

An excellent overview of the RESS process, including the fluid mechanics of the subsonic and supersonic flows, is provided by Weber and Thies[5] and earlier by Debenedetti and colleagues.[6] These authors have borrowed results from the ideal gas free-jet literature and utilized quasi-1-D (QOD) analysis of the free-jet as an approximation to understand the RESS expansion for supercritical fluids. In this article we present numerical results for the axisymmetric, 2-D, free-jet (ASFJ) expansion with a Redlich-Kwong equation of state, which incorporates the repulsive potential excluded volume and the attractive potential real gas effects, and is a first approximation for many SCFs. We also present experimental data for supercritical CO_2 expansions, which compares reasonably well with our calculations for the jet structure. The expansion is directed at a flat plate, to simulate the use of RESS to grow thin films. We find that the QOD analysis and the ideal gas approximation do in fact provide reasonable first approximations to the flow properties.

Correspondence concerning this article should be addressed to D. R. Miller at dmiller@ucsd.edu.
Current address of I. Khalil: Sandia National Laboratories, Albuquerque, NM; e-mail: ikhalil@sandia.gov.

We have primarily studied the free-jet expansion of pure CO_2 originating from small orifices rather than capillary tubes in order to reduce the effects of viscosity, heat transfer, and clustering or condensation in the subsonic flow. The subsonic expansion from stagnation to sonic conditions in the orifice flow is essentially inviscid and adiabatic, hence, isentropic, which provides a well defined inlet boundary condition for our free-jet calculations and for our experiments. In the later sections we first briefly discuss the equations and our numerical method, and then the experimental methods and results. Additional details are available elsewhere.[7]

Theory and Numerical Calculations

For ideal gases, there have been many rigorous calculations of axisymmetric free-jet supersonic expansions.[4,8] Although the method of characteristics is regarded as the most accurate for the isentropic supersonic free-jet expansion, the time-dependent methods are useful to correctly capture shock wave structure and to include kinetic effects,[9] and they can be extended to the viscous subsonic flow. Many texts provide recipes and summarize the advantages and disadvantages of various numerical methods applicable to the free-jet supersonic expansion.[10] One of the difficulties of incorporating real gas effects into the supersonic compressible flow calculation is the need to calculate the speed of sound at each grid point and time step, especially important in methods which incorporate compression and rarefaction waves, such as the flux splitting Godunov type methods. Often for hypersonic nozzles, wherein flows originate from high temperature and pressure, it is sufficient to consider only the excluded volume repulsive potential correction to ideal gas behavior.[11] However, since the SCF flows of interest here originate from high pressure and sufficiently low temperatures, it is necessary to consider both the excluded volume and the attractive potential corrections to ideal gas behavior. We have chosen the finite difference, two-step Lax-Wendroff method, because it is suitable for the hyperbolic partial differential equations of the free-jet, it has been utilized successfully for ideal gas free-jet expansions, the real fluid equations of state are easily incorporated, and the speed of sound enters explicitly only in the stability criteria for the time increment.[12] We begin by studying free-jet expansions for pure supercritical CO_2 because it is a well studied fluid in both the molecular beam field, under ideal gas conditions, and in the SCF field as an important supercritical solvent. Furthermore, CO_2 has been characterized by several equations of state for which the interaction parameters are well determined in the literature.[13,14]

The time-dependent partial differential equations to be solved for the inviscid, adiabatic, axisymmetric free-jet supersonic expansion (ASFJ) are well established[8,15] and are given in conservation form in Eqs. 1

$$\frac{\partial E}{\partial t} + \frac{\partial F}{\partial x} + \frac{\partial G}{\partial r} + \frac{H}{r} = 0 \tag{1}$$

$$E = \begin{vmatrix} \rho \\ \rho u \\ \rho v \\ \rho[e + 1/2(u^2 + v^2)] \end{vmatrix}$$

$$F = \begin{vmatrix} \rho u \\ \rho u^2 + P \\ \rho u v \\ u\{\rho[e + 1/2(u^2 + v^2)] + P\} \end{vmatrix}$$

$$G = \begin{vmatrix} \rho v \\ \rho u v \\ \rho v^2 + P \\ v\{\rho[e + 1/2(u^2 + v^2)] + P\} \end{vmatrix}$$

$$H = \begin{vmatrix} \rho v \\ \rho u v \\ \rho v^2 \\ v\{\rho[e + 1/2(u^2 + v^2)] + P\} \end{vmatrix}$$

In addition, two equations of state are required, $e(\rho,T)$ and $P(\rho,T)$, to complete the set of six equations and six unknowns, with velocity components u and v in the axial and radial directions, respectively, pressure P, temperature T, density ρ, and the internal energy per unit mass e. We also use enthalpy $h(\rho,T) = e + P/\rho$, to compute $e(\rho,T)$, and entropy $s(\rho,T)$, for isentropic calculations. Except near solid boundaries and in the jet boundary shear layers, the neglect of viscosity and heat conduction is a good approximation. For the SCFs and conditions considered here, the more serious approximation is that we assume a homogeneous fluid, neglecting clustering and condensation effects. The numerical method can incorporate such kinetics, however, we defer such analysis to a future publication.

We have studied several equations of state in our calculations, including Redlich-Kwong and Peng-Robinson cubic equations,[16] as well as Huang et al.'s 27-parameter equation,[17] and we previously showed that they provide similar results for CO_2.[7,18] Although the temperature-dependent parameters make the Peng-Robinson and 27-parameter equations of state more rigorous, especially at higher pressures, the axisymmetric results presented here primarily use the simple Redlich-Kwong cubic equation of state

$$P = \frac{RT}{v - b} - \frac{a}{T^{1/2} v(v + b)} \tag{2}$$

$$a = 0.42784 \frac{R^2 T_c^{2.5}}{P_c} \text{ and } b = 0.08664 \frac{RT_c}{P_c}$$

The cubic equations of state are readily adaptable to many mixtures of solutes with solvents, they have been well studied by chemical engineers, and the mixture interaction parameters are available.[13,14] Calculations of e, h, and s are taken from standard texts.[16] As an example, the Redlich-Kwong relation for h becomes

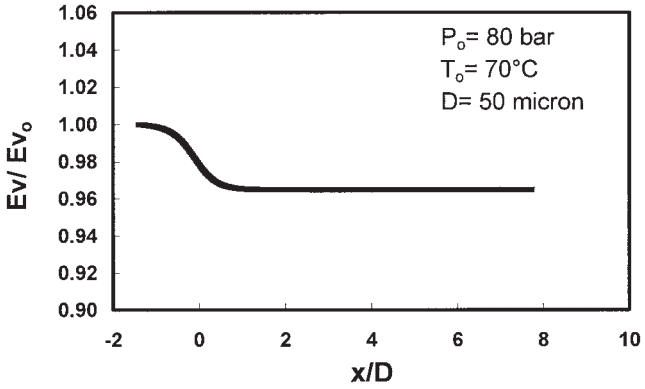

Figure 1. Vibrational relaxation of CO_2.

$$h = h_{IG} + h_R = h_{IG}(T) + RT\left[\frac{3a}{2bRT^{3/2}}\ln(1 + b/v) - \frac{Pv}{RT} + 1\right] \quad (3)$$

where $h_{IG}(T)$ is the ideal gas contribution and h_R the residual real gas correction term. We evaluated the consistency of our thermodynamic numerical subroutines by verifying that exact relations, such as $dh = Tds + dP/\rho$ were accurate to within 0.1% over the range of conditions encountered in our expansions.

Over the range of temperatures encountered in our supercritical CO_2 expansions, below 70°C, only the degenerate $\nu_2 = \nu_3$ bending modes of CO_2 are excited. At 70°C, only 6% of the molecules are in the first excited state of this bending mode. Therefore, in addition to the use of an empirical heat capacity[19] $Cp(T)$ to determine Δh_{IG}, we have used the rigorous statistical mechanics relations[20] to incorporate the contribution to h, s, and e of these modes for most of our calculations, and in particular to establish the inlet conditions to the free-jet expansion.

Furthermore, there are not sufficient collisions in the flow to maintain vibrational equilibrium, so that these bending modes freeze out near the exit of the orifice and inlet to the free-jet expansion. An example of this is shown in Figure 1 where we plot the vibrational energy normalized by the initial vibrational energy Ev/Ev_o, as a function of axial distance, measured in nozzle throat diameters, with $(x/D) = 0$ at the throat. We have integrated the vibrational relaxation equation for the CO_2 bending mode,[9] using flow properties from a QOD nozzle approximation, discussed later, for the SCF expansion from stagnation conditions at 70°C and 80 bar into the supersonic free-jet. The relaxation equation is

$$\frac{dE_v}{dt} = \frac{E_{v,eq} - E_v}{\tau} \quad (4)$$

where the relaxation time τ is taken from Anderson[21]

$$\log(\tau P)_{CO_2—CO_2} = 17.8(T^{-1/3}) - 1.808 \quad (5)$$

As shown in Figure 1, the vibrational energy freezes rapidly beyond the sonic throat. Therefore, a reasonable approximation for the supercritical CO_2 free-jet expansion is to include only the classically excited translation and rotation degrees of freedom, which provides a constant heat capacity $Cp = 3.5R$ and $h_{IG} = 3.5RT$. For this reason, it is also appropriate to compare our Redlich-Kwong free-jet results with the well established ideal gas $\gamma = 1.4$ free-jet results.

The speed of sound $c(\rho,T) = (dP/d\rho)_s^{1/2}$ enters explicitly into the calculation as a stability constraint on the time step. In order to achieve the accuracy required, using any of our equations of state, we numerically evaluated the derivative $(dP/d\rho)_s$ at any ρ and T by selecting a small $\Delta\rho$ about the local ρ and calculating the associated ΔP for an isentropic process using both $P(\rho,T)$ and $s(\rho,T)$ equations of state.

The rectangular mesh we have used is shown in Figure 2 for a typical calculation, with a plate at 9.4 orifice dia., D, from the orifice exit. The grid is 226 × 240 points. The indices i and j denote equally spaced grid points in the axial and radial directions, respectively ($\Delta x = \Delta r = D/24$). The numerical algorithm could be adjusted for an arbitrary plate location, which we have varied from $Xp/D = 5$ to 15. The first 12 grid points on the lefthand side of the grid correspond to the orifice exit where the free-jet flow begins. To avoid the singularity of the differential equations, we shift the grid points nearest to the axis of symmetry by $\Delta r/2$ from the exact location of the axis. The inlet conditions for the free-jet are established for all the variables, assuming $v = 0$, by an exact isentropic calculation from stagnation conditions (P_o, T_o, h_o, s_o) to sonic conditions at the orifice exit. This requires the simultaneous solution of three equations: $h(\rho,T) + u^2/2 = h_o(\rho_o,T_o)$; $s(\rho,T) = s_o(\rho_o,T_o)$; and $u = c(\rho,T)$ for the three unknowns ρ, T, and u, at the sonic point. To keep the calculation consistent, we use the same equation of state for this initial part of the expansion as we use for the free-jet. Since the Redlich-Kwong equation becomes poor at higher pressures an alternative approach would be to use a more rigorous equation for this initial subsonic flow and then switch to the simpler Redlich-Kwong or Peng-Robinson for the supersonic free-jet flow. Together with the exit orifice diameter, this calculation also provides the flow rate which can be experimentally measured in order to verify the calculation. We have shown previously that our computed flow rates are in good agreement with the measured flow rates.[7,18] We have assumed no streamline curvature at the inlet to the free-jet, which is an approximation best achieved by a short converging nozzle.[22]

The two-step Lax-Wendroff approach we have used is taken from Sinha et al.[15] as modified by Forney.[23] We assume that the

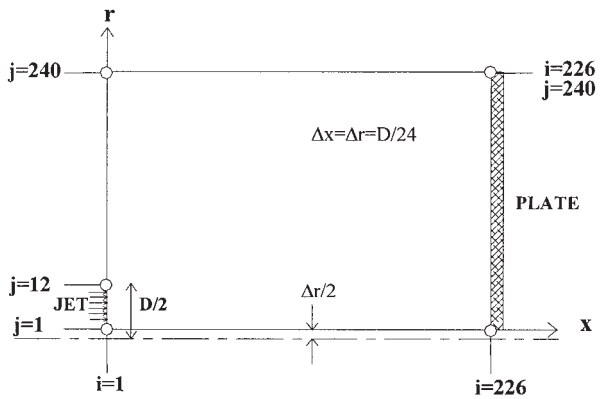

Figure 2. Rectangular computational grid.

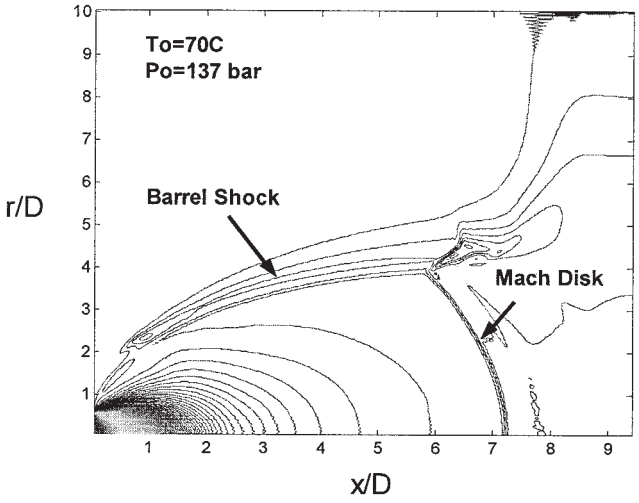

Figure 3. CO_2 Computed density contours.

flow properties at time t are known and we use a Taylor series expansion in time to get the new flow field at $t+\Delta t$.

A full time step is used in the predictor step with forward differencing

$$E^p(x, r, t+\Delta t) = E^*(x, r, t) - \frac{\Delta t}{\Delta x}[F(x+\Delta x, r, t) - F(x, r, t)] - \frac{\Delta t}{\Delta r}[G(x, r+\Delta r, t) - G(x, r, t)] - \frac{\Delta t}{r} H(x, r, t) + S(x, r, t) \quad (6)$$

where E^* is a spatial smoothing term

$$E^*(x, r, t) = 1/4\,[E(x+\Delta x, r, t) + E(x-\Delta x, r, t) + E(x, r+\Delta r, t) + E(x, r-\Delta r, t)] \quad (7)$$

and S is an artificial, numerical viscosity term suggested by Anderson[24]

$$S(x, r, t) = \frac{C_x|P(x+\Delta x, r, t) - 2P(x, r, t) + P(x-\Delta x, r, t)|}{P(x+\Delta x, r, t) + 2P(x, r, t) + P(x-\Delta x, r, t)} \times [E(x+\Delta x, r, t) - 2E(x, r, t) + E(x-\Delta x, r, t)] + \frac{C_y|P(x, r+\Delta y, t) - 2P(x, r, t) + P(x, r-\Delta y, t)|}{P(x, r+\Delta y, t) + 2P(x, r, t) + P(x, r-\Delta y, t)} \times [E(x, r+\Delta y, t) - 2E(x, r, t) + E(x, r-\Delta y, t)] \quad (8)$$

Cx and Cy are two arbitrarily specified parameters with typical values ranging from 0.01 to 0.3.

We have followed Forney[23] in using the spatial smoothing term because we are not able to achieve convergence to a stable solution using only numerical viscosity for our free-jets. Therefore, in our numerical code, in the initial time steps we use only this smoothing term, and then only use the artificial viscosity in the final iterations to improve the accuracy of the solutions. A full time step is used in the corrector step with backward differencing. Each step is first-order accurate since the expansion contains only first-order terms in the relevant Taylor series. It becomes second-order accurate with the addition of the second step. This reduces the amount of computing time, while maintaining the accuracy of the computation. The details are given elsewhere.[7]

Referring to Figure 2, the inflow sonic boundary conditions are applied at grid points that correspond to the orifice diameter. The boundary conditions on all grid points above the orifice are based on ambient conditions, with zero velocity in both axial and radial directions.[15] For the top boundary, the velocity in the radial direction is calculated by linear extrapolation using the two adjacent interior grid points, the velocity in the axial direction is set equal to zero, and ambient conditions are used for pressure and temperature. The reflection technique[25] is used for the right hand side at the plate, and symmetry boundary conditions are used along the centerline.

The method is explicit, which means that the time step used in the calculation can not be arbitrarily chosen, but is constrained by stability requirements. The Courant-Friedrichs-Lewy (CFL) criteria for stability is used to calculate the time step[12]

$$\Delta t < \frac{\Delta x \Delta y}{|u|\Delta y + |v|\Delta x + c\sqrt{\Delta x^2 + \Delta y^2}} \quad (9)$$

Because the speed of sound varies rapidly for the SCFs under our expansion conditions, we found it necessary to calculate the maximum Δt at each grid point at the end of each time step iteration, and then to select the minimum value from the entire set to be used as the new time step for the next iteration.

Initial conditions for ρ, u, v, P, T and e, for all the grid points, were required in order to start the finite-difference solution. Although, the steady-state solution of CO_2 is independent of initial conditions, we found that there is a narrow range of acceptable values for which convergence could be achieved with these real fluid equations of state. After various attempts we found that suitable initial conditions came from the steady-state solution of the ideal gas. The process of obtaining a solution for an axisymmetric free-jet using a cubic equation of

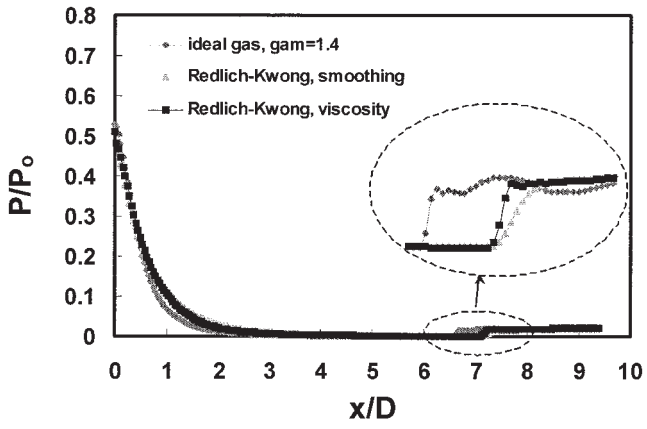

Figure 4. Centerline pressure vs. x/D (CO_2, P_o= 137 bar, T_o= 70°C).

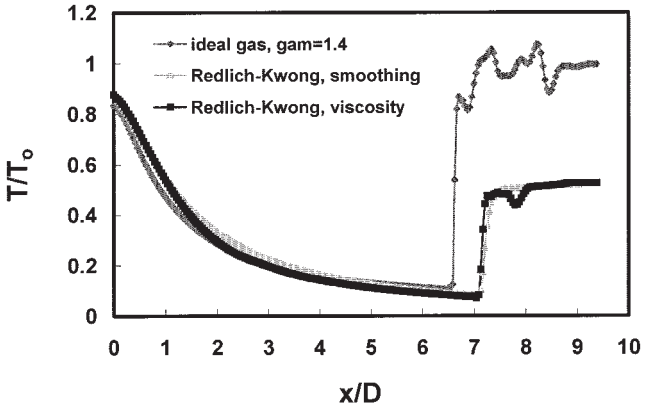

Figure 5. Centerline temperature vs. x/D (CO_2, P_o= 137 bar, T_o= 70°C).

state, such as the Redlich-Kwong equation, therefore, consisted of three steps. A typical calculation involved 2,000 time steps using the ideal gas equation of state, to obtain initial conditions at all grid points for Redlich-Kwong. Then, the Redlich-Kwong equation of state was introduced, together with the smoothing term, and another 2,000 time step iterations were computed. Finally, the artificial viscosity term was added and run for an additional 1,000 time steps. One such run of about 5,000 time steps, for one given source condition, typically required 3 h on a Dell PC with a P4 CPU 1.80 GHz at 1 GB RAM, programmed in FORTRAN 90.

Figure 3 is an example of the computed density profiles for the expansion of supercritical CO_2 from 137 bar, 70°C, impacting a vertical plate at Xp/D = 9.4 source diameters downstream from the sonic source.

Figures 4 and 5 show pressure and temperature profiles along the jet axis for three calculations: Redlich-Kwong results using only the smoothing routine; Redlich-Kwong results corrected with the numerical viscosity; and for comparison an ideal gas, γ = 1.4, result. We have shown elsewhere that the Peng-Robinson equation gives very similar results.[7] We have also verified that this ideal gas result from our time-dependent method agrees very well, to within 3%, with the exact method of characteristics for the ideal gas in the isentropic region upstream of the shock.

We find that the axial shock, called the Mach disk, and flow properties are more accurately defined by including the numerical viscosity but oscillations persist downstream of the shock, a trade-off between accuracy and a dampening of the numerical oscillations. It is clear that the most significant real gas effect is on the temperature downstream, of the shock, a result expected by analogy with the thermodynamic Joule-Thompson effect. Temperature is a serious issue for clustering and growth in RESS experiments since solute solubility is very sensitive to temperature. Interestingly, the ideal gas approximation is a reasonable first approximation for the shock location and pressure profiles. As we show later, these results for the jet shock structure agree well with experiment.

The quasi-1-D equations are routinely used in compressible flow to study subsonic-to-supersonic expansions in converging-diverging nozzles where a physical nozzle area A(x) is prescribed.[26] The equations are quasi-1-D because the properties are assumed to change only in the flow coordinate *x* along the nozzle centerline, and to be constant normal to this direction. The QOD equations are obtained rigorously from the exact axisymmetric equations by integrating over the direction normal to the centerline and can be easily solved as exact algebraic equations, or with the same time-dependent Lax-Wendroff method.[24] Unfortunately the free-jet has no nozzle boundary so the area A(x) is not prescribed. For ideal gases all flow properties can be expressed as a function of Mach number and specific heat ratio, γ, so that a common approach for ideal gases has been to solve the ASFJ problem for Mach number along the centerline, and then use these rigorous results to work backward with the QOD equations to identify an effective A(x), which will mimic the ASFJ. For SCFs the Mach number is not a unique parameter to characterize the flow properties and we, therefore, have identified stream tubes from our ASFJ calculations to determine an effective A(x). Figure 6 shows the area profile, normalized by the sonic or throat area, for both the ideal gas γ =1.4 isentropic expansion result and the area ratio extracted from our ASFJ calculations for supercritical CO_2 at two-source pressures. The latter are obtained by tracing a streamline back from the Mach disk to the inlet, thus defining a stream tube or effective diverging nozzle contour in which the central core of the expansion occurs. Interestingly, using this method we find from our calculations that only about 25% of the total flow passes through the Mach disk. This agrees qualitatively with the estimates of Weber and Thies,[5] based on ideal gas expansions.

Although there is some pressure dependence, we see that the effective QOD areas A(x) are quite similar. This result suggests that the A(x) determined by the well known ideal gas γ =1.4 correlations,[4] and used as an approximation by several researchers, provides a reasonable expansion ratio for supercritical CO_2 in which to explore thermodynamic and kinetic effects. We now proceed to compare our ASFJ calculations with experimental data.

Experimental Apparatus and Results

We briefly describe here the principle components of the experimental setup and a few examples of the experimental results to demonstrate the usefulness of the calculations. The CO_2 delivery system was standard using an ISCO pump and Omega strain gauge pressure transducers. The setup and shadowgraph is shown in Figure 7.

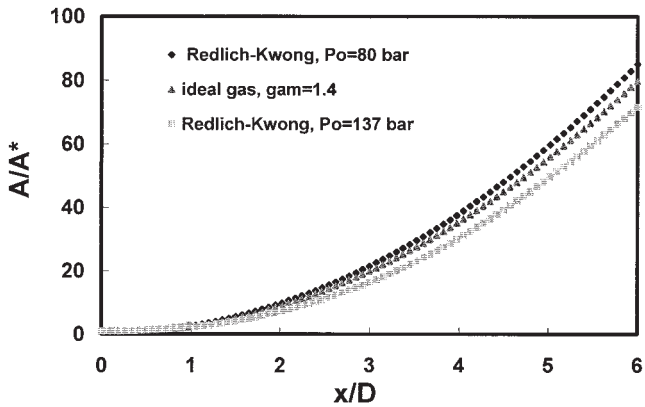

Figure 6. Effective Quasi-1-D Nozzle Area - A/A* vs. x/D.

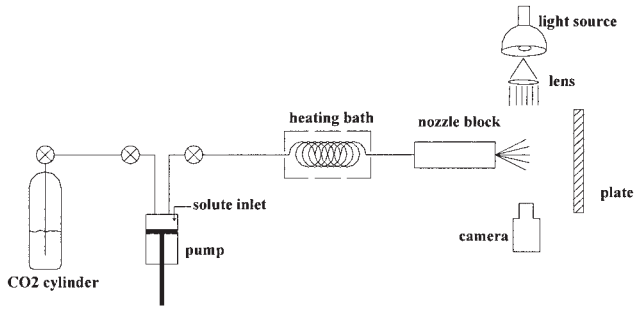

Figure 7. Setup and shadowgraph.

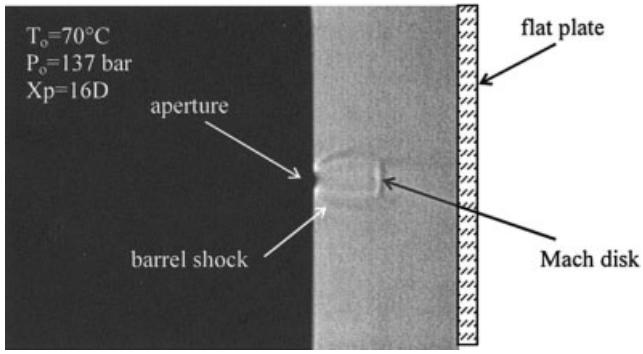

Figure 8. CO_2 Free-Jet shadowgraph.

The small nozzle orifices were made by drilling an aperture into the face of a commercial 1/8 in. stainless steel swagelok cap fitting. The nozzles were mounted into a small stainless steel block with a thermocouple inserted directly into the stagnation chamber, just upstream of the aperture. Heat transfer is negligible in such short nozzles so that the flow is adiabatic. We verified this by comparing runs with the nozzles completely emerged in a constant temperature bath to runs with the nozzle suspended in the ambient air. The CO_2 was preheated in a water bath and then controlled by a small resistive heater in the nozzle block assembly. Nozzle diameters were calibrated *in situ* by measuring the flow rates for ideal gas argon expansions, for which the equation of state is exact, and comparing with exact calculations. Using these flow diameters, we also find good agreement of our measured CO_2 flow rates with the isentropic flow calculations using the Redlich-Kwong equation of state.[7,18] We, therefore, have confidence that the inlet boundary conditions for the free-jet are consistently established both for our calculations and for our experiments, except for the assumption of no streamline curvature.

We have primarily studied flows from two orifice diameters, 100 μm and 50 μm. The pumping capacity permitted us to reach 100 bar with the 100 μm orifice and 200 bar with the 50 μm orifice. While we are able to vary temperature the experiments reported here are all close to 70°C. All source conditions were above the critical point, and chosen so that both the entropy and the specific volume exceeded the critical point values throughout the expansion.

The shadowgraph method[27] used a lamp light source, a 10 cm diam. planar-convex lens, and a computer coupled digital Nikon camera with a 28–108 mm zoom lens with a maximum f/3.5 aperture. The spatial resolution was calibrated with micrometers. The technique is sensitive to the spatial second derivative of density, and a typical photo is shown in Figure 8. The side barrel shock and axial Mach disk shock structure of the flow is easily observed and very close to the calculated structure. From such shadowgraph photos the position $(x/D)_{MD}$ of the Mach disk shock waves can be measured to within 0.25 orifice dia. To verify the accuracy of our measurements, we previously compared results for the Mach disk location for argon expansions into atmosphere, no plate, with well established ideal gas results.[7,18] Insertion of a flat plate moves the normal shock wave closer to the source. Figure 9 shows experimental data for the shock position as a function of the plate position for CO_2, together with our numerical results, for the 50 μm orifice. It is clear that the Redlich-Kwong CO_2 numerical calculations provide reasonable results for the shock position.

Pressure data at the plate was obtained by mounting an Omega strain gauge pressure transducer near the plate surface behind a 100 μm aperture, so that the resolution is only one or two nozzle diameters. Figure 10 shows examples of two pressure profiles, data and calculated results. The calculated profiles appear reasonable. While not shown here, the comparisons become worse at much higher-pressures, where condensation was in fact readily observed downstream of the Mach disk, in the subsonic flow impacting the plate.[7] As we stated earlier, these calculations have ignored condensation effects altogether, even though the expansion proceeds well into the two-phase region for CO_2. At the lower-pressures shown in Figure 10 the agreement is good, and might require the addition of viscous effects to be improved.

Quantitative temperature measurements on the plate, are difficult because of probe and plate heat-transfer effects. Figure 11 shows a best and a worse case agreement for temperature profiles on the flat plate. The temperatures were taken with a thermocouple placed flush with the surface. Even the low-pressure case is not well reproduced by these calculations which neglect heat transfer to and within the plate. Not only is the magnitude underestimated but the predicted drop outside about five diameters is not measured. As with the pressure data, the agreement becomes even worse at higher pressures because of the onset of condensation effects and the associated heat release, and likely also because the Redlich-Kwong equation is not adequate.

It is difficult to make quantitative temperature measurements within the free-jet, not only because of probe heat transfer

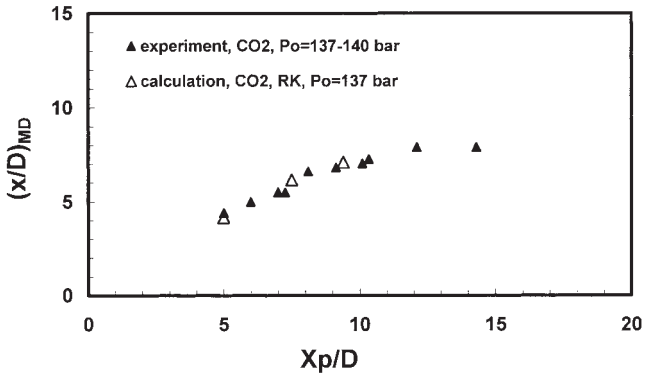

Figure 9. Mach disk Location as function of plate distance.

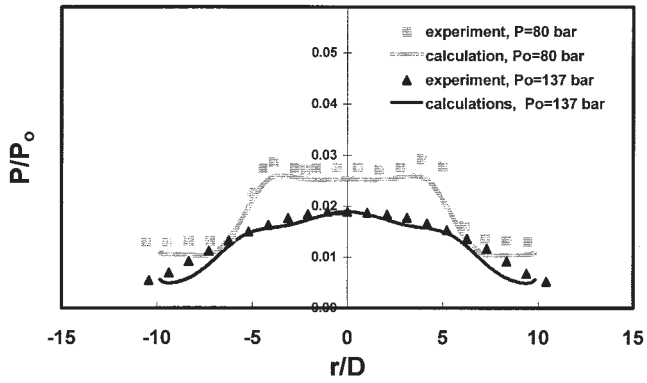

Figure 10. Pressure at the plate.

effects, and the small physical scale of these experiments with supercritical CO_2, but because in the supersonic regime the probe induces bow shocks in front of the thermocouple probe itself. Figure 12 shows a probe temperature profile obtained by moving a small 100 μm diam. thermocouple junction, approximated as a small sphere suspended on two 50 μm wires from the rear, into the free-jet (no plate) and along the jet axis. The shadowgraph camera probe was used to examine the distances and to observe the bow shock, which typically was less than x/D = 0.25 in front of the thermocouple probe when the probe penetrated upstream of the Mach disk. The CO_2 expansion is from 70°C and 80 bar through the 100 μm orifice, and the Mach disk is at x/D = 5.8. The position of the Mach disk was measured before the probe was inserted and is indicated as a reference. We have not made any corrections for probe heat-transfer effects to the subsonic flow around the thermocouple. The calculated points upstream of the Mach disk assume the probe temperature would be close to the fluid temperature just downstream of the induced bow shock along the jet axis. Using the experimental bow shock location, we used our ASFJ calculations to obtain the flow properties before and just after the shock; we did not solve for the 2-D flow downstream of the bow shock and around the probe. In the subsonic flow downstream of the Mach disk we assumed the probe reflected the numerically calculated local fluid temperature along the jet axis. The details of this experiment are available elsewhere.[7] Clearly the data and calculations have several caveats but other than the displacement in axial position, which we do not yet

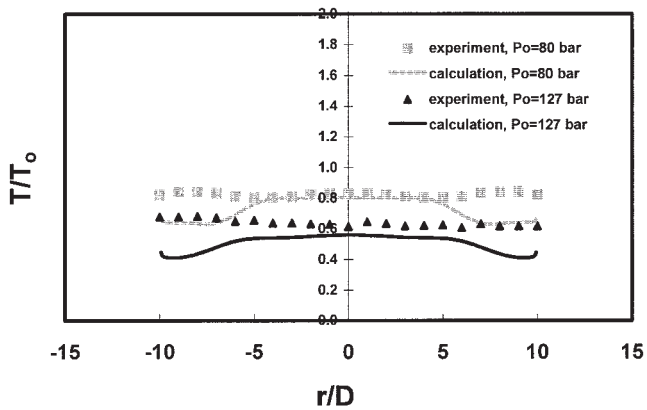

Figure 11. Temperature at the plate.

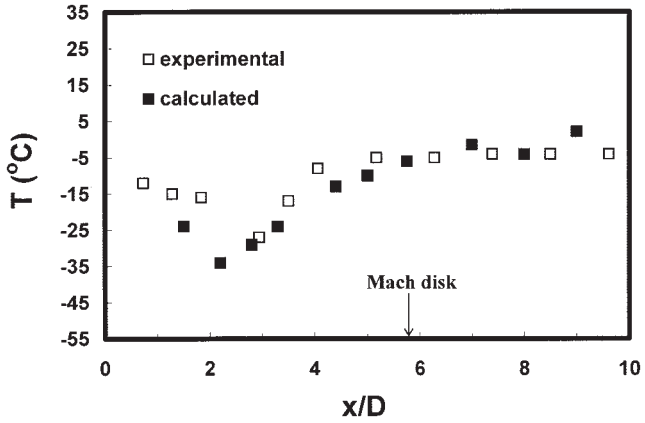

Figure 12. Probe temperature of CO_2 free-Jet into atmosphere (P_o= 80 bar, T_o= 70°C).

understand, the data appear to support the numerical calculations. The comparison would be worse at higher-pressures where the Redlich-Kwong or Peng-Robinson equations may not be appropriate, and where cluster formation begins to occur. If the fluid were an ideal gas then, under the assumptions we have made the probe temperature would always be close to the stagnation temperature of 70°C.

In conclusion, we have been able to extend a standard time marching, compressible flow calculations to nonideal gases, using reasonable equations of state which model supercritical CO_2 RESS experiments. Since these supersonic expansions extend into the thermodynamic two-phase regimes, and we have used the simplest equation of state, neglecting any kinetic or thermodynamic condensation considerations, it is surprising and interesting that the results seem to compare reasonably well with the experiments, except at the highest pressures. We are able to show that the quasi-1-D and ideal gas approximations often used by RESS investigators are quite reasonable first approximations. In particular it appears useful to use the QOD calculations based on an ideal gas nozzle area ratio and, as a first approximation, to insert the shock wave at a position predicted by ideal gas correlations. To improve these calculations we need to consider the effects of condensation, and heat conduction and viscosity at the plate. While other equations of state would be more rigorous, and can be incorporated into our calculations, the simple cubic equations we have used can be easily extended to solute mixtures of interest to chemical engineers.

Literature Cited

1. Matson D, Peterson R, and Smith R. Production of powders and films by the rapid expansion of supercritical solutions. *J. Materials Sci.*. 1987; 22:1919-1928.
2. Arai Y. *Supercritical Fluids: Molecular Interactions, Physical Properties, and New Applications*. New York: Springer, 2001.
3. Sun Y. *Supercritical Fluid Technology in Materials Science and Engineering*. New York: Marcel Dekker, 2002.
4. Miller DR. Free jet sources. In: Scoles G, *Molecular Beam Methods*. New York: Oxford University Press, 1988:14-53.
5. Weber M, Thies M. Understanding the RESS Process. In: Sun Y, *Supercritical fluid technology in materials science and engineering*. New York: Marcel Dekker, 2002:387-437.
6. Kwauk X, Debenedetti P. Mathematical Modeling of Aerosol Forma-

tion by Rapid Expansion of Supercritical Solutions in a Converging Nozzle. *J. Aerosol Science*. 1993;24:445-469.
7. Khalil I. PhD thesis. *Free-Jet Expansion of Supercritical CO_2*. University of California, San Diego, 2003.
8. Saito T, Nakatsuji H, Teshima K. Numerical simulation and visualization of free-jet flow fields. Trans. *Jpn. Soc. Aero. Space Science*. 1986;28: 240-258.
9. Anderson JD. A Time dependent analysis for vibrational and chemical nonequilibrium nozzle flows. *AIAA J*. 1970;8:545-550.
10. Chung TJ. *Computational Fluid Dynamics*. Cambridge: Cambridge University Press, 2002.
11. Candler G. Hypersonic nozzle analysis using an excluded volume equation of state. University of Minnesota. Private conversation.
12. Hirsch C. *Numerical Computation of Internal and External Flows*. New York: John Wiley & Sons Ltd., 1990.
13. Clifford T. *Fundamentals of Supercritical Fluids*. Oxford Science Publications, 1999.
14. Poling BE, Prausnitz JM, O'Connell JP. *The Properties of Gases and Liquids*. New York: McGraw Hill, 2000.
15. Sinha R, Zarkay V, Erdos J. Flowfield analysis of plumes of two-dimensional underexpanded jets by a time-dependent method. *AIAA J*. 1971;9:2363-2369.
16. Sandler SI. *Chemical and Engineering Thermodynamics*. New York: John Wiley & Sons, Inc., 1999.
17. Huang F, Li M, Lee L, Starling K. An accurate equation of state for carbon dioxide. *J. of Chem. Eng. of Japan*. 1984;18:490-495.
18. Khalil I, Miller DR. The Interaction of a supercritical fluid free-jet expansion with a flat surface. Proc. 6th International Symposium on Supercritical Fluids. Versailles, France. 2003;1:655-660.
19. Wark K. *Advanced Thermodynamics for Engineers*. New York: McGraw-Hill, 1995.
20. Hecht C. *Statistical Thermodynamics and Kinetic Theory*. New York: Dover Publications, 1990.
21. Anderson JD. A Time dependent quasi-one-dimensional analysis of population inversions in an expanding gas. *NOLTR* 69-200, 1969.
22. Murphy H, Miller DR. Effects of nozzle geometry on kinetics in free-jet expansions. *J. Phys. Chem*. 1984;88:4474-4478.
23. Forney LJ. Particle impaction in axially symmetric supersonic flow. *J. Aerosol Sci. and Technol*. 1991;15:49-59.
24. Anderson JD. *Computational Fluid Dynamics, The Basics with Applications*. New York: McGraw-Hill, 1995.
25. Moretti G. The Importance of Boundary Conditions in the Numerical Treatment of Hyperbolic Equations. PIBAL Report 68-34. New York: Polytechnic Institute of Brooklyn, 1968.
26. Anderson JD. *Modern Compressible Flow, with Historical Perspective*. New York: McGraw-Hill, 1990.
27. Liepman HW, Puckett AE. Introduction to Aerodynamics of a Compressible Fluid. New York: John Wiley & Sons Ltd., 1947.

Manuscript received Nov. 13, 2003, and revision received March 22, 2004.